Research Article GU J Sci, Part A, 10(3): 327-340 (2023) 10.54287/gujsa.1294774

Gazi University
Journal of Science
PART A: ENGINEERING AND INNOVATION
http://dergipark.org.tr/gujsa

Optimization of Green Synthesis Parameters of Silver Nanoparticles with Factorial Design for Dye Removal

Gülçin DEMİREL BAYIK[1*] Busenur BAYKAL[1]

[1]*Zonguldak Bulent Ecevit University, Department of Environmental Engineering, Zonguldak, Türkiye*

Keywords

Silver Nanoparticles
Factorial Design
Green Synthesis
Dye Removal
Adsorption

Abstract

In this study production of silver nanoparticles (AgNPs) from collard greens were optimized by the design of experiments (DOE). A 2^4 full factorial design was employed to evaluate the effects on two responses. The optimized values for AgNP production were 1:7 leaf to water, 1:4 extract to $AgNO_3$, 5 molar $AgNO_3$, and a leaf size of <1 mm. For dye removal efficiency, the optimized values were changed to 1:15 of leaf to water and 1:10 of extract to $AgNO_3$, while the other two parameters remained the same. SEM (scanning electron microscopy) showed that optimizing the process for dye removal led to smaller AgNP production with increased surface area, resulting in higher absorbency. ANOVA (analysis of variance) tables were used to interpret each parameter's main and effects on interaction. Additionally, reaction rate kinetics were estimated, and dye removal showed a slightly higher R-square of pseudo second-order than NP production, which fits the pseudo first-order reaction model.

Cite

Bayık, G. D., & Baykal, B. (2023). Optimization of Green Synthesis Parameters of Silver Nanoparticles with Factorial Design for Dye Removal. *GU J Sci, Part A, 10*(3), 327-340. doi:10.54287/gujsa.1294774

Author ID (ORCID Number)

0000-0002-5761-5327 Gülçin DEMİREL BAYIK
0000-0002-6111-3303 Busenur BAYKAL

Article Process

Submission Date 09.05.2023
Revision Date 04.07.2023
Accepted Date 07.08.2023
Published Date 26.09.2023

1. INTRODUCTION

Nanotechnology refers to the process of creating and manufacturing materials and technologies at the nanoscale. The fabrication of nanoparticles utilizing various metals, including zinc oxide, copper oxide, gold, and silver is one of the most exciting fields of nanotechnology study. By precisely controlling the size, shape, and chemical composition of nanoparticles, scientists can produce distinct materials with tailored properties suitable for various applications. This innovative technology is advancing rapidly and has the potential to revolutionize various industries (Golli et al., 2023). Silver nanoparticles (AgNPs) have gained substantial interest in different research areas with their outstanding electrical conductivity, catalytic characteristics, and antibacterial capabilities (Min et al., 2023).

AgNPs can be produced in several ways, involving physical, chemical, and biological methods. Because of its environmentally benign and sustainable approach, green synthesis for AgNPs has been an important research subject in the field of AgNP synthesis. This approach has various advantages, including low energy usage and the use of mild reaction conditions, making it a preferred choice among researchers (Nie et al., 2023). Plants are one of the biological agents used in the green synthesis of NPs. Due to their natural phytochemical structure, which includes terpenes, flavonoids, and antioxidants that play role in reducing process for nanoparticle production (Jeevanandam et al., 2016).

Nanoparticles posess a variety of physicochemical features, including an increased surface-to-volume ratio, smaller size, catalytic potential, thermal and electrical conductivity, and optical absorption. Catalysts, active food packaging materials, environmental remedies, antimicrobial activity, filters, chemical sensors, medical

*Corresponding Author, e-mail: gulcin.demirel@beun.edu.tr

imaging, and nanocomposites can all be made from metal nanoparticles with adjustable sizes, shapes, and compositions (Iravani, 2011; Silva et al., 2015; Rastogi et al., 2017). Silver nanoparticles (AgNPs) constitute a common type of metal nanoparticle used in cosmetics, water treatment, medicine, and pharmaceuticals (Rastogi et al., 2017).

Environmental applications for nanomaterials include removing bacteria, heavy metals, and aromatic polycyclic hydrocarbons (PAHs), the degradation of carbon tetrachloride, a key function in the desulfurization process, and the remediation of pesticides, chlorinated organic solvents, and dye-contaminated water bodies (Kumar Das et al., 2022). Among numerous water pollutants, chemical dyes are a significant contributor to industrial water pollution and a significant environmental risk. Three common water contaminants have been recognized as carcinogenic and mutagenic: Congo red (CR), Rhodamine B (RhB), and Methylene blue (MB). MB becomes absorbed in suspended particles and is unable to evaporate or decompose in water, although it does not bioaccumulate in aquatic animals, according to the US Environmental Protection Agency (EPA) (Ngoc et al., 2022). Synthetic dyes deriving from different industries like textile, plastic, paper, and food industries are treated by conventional methods such as adsorption, advanced oxidation, photocatalytic oxidation, radiation, and membrane separation (Wang et al., 2018; Jiang et al., 2019; David & Moldovan, 2020). Among these methods, the adsorption method is well known for being advantageous because it is cost-effective and easy to manage (Çimen et al., 2019; Yaghoobi et al., 2023). Choosing a high-performance adsorbent is critical to achieving a successful and effective adsorption process. A recent study indicates that porous metal oxides are effective solid adsorbents for water contaminants. These materials are advantageous in adsorption process because they have a large surface area and they have many chemically active sites, and functionalization capability (Lee et al., 2013).

In this study, design of experiments (DOE) has been used as a method to assess the effects of two optimization conditions on the two responses, namely NP production quantity and dye removal efficiency. The synthesis of AgNPs was accomplished by reacting collard green leaf (*Brassica oleracea acephala*) with $AgNO_3$ to reduce silver ions. A two-level full factorial design (FFD) was employed, where all possible combinations of parameter levels were examined to analyze the results.

2. MATERIAL AND METHOD

Experimental Design

The experimental program was created using a full factorial design with three replicates. The the influence of four distinct parameters on the amount of produced Ag nanoparticles (AgNP) was investigated. Minitab 18 statistical software was used to design and analyze the process. Four parameters with two levels were used in the design. The parameters were the ratio of water to plant leaf (LW) in the extraction stage, the ratio of extract to $AgNO_3$ (EAgNO3), the molarity of AgNO3 (Mol), and the plant leaf size (LS). Response factors were selected as the amount of AgNPs synthesized (g) and dye removal efficiency (%). A total of 48 experiments with 3 replicates were designed with the two levels are shown in Table 1.

Table 1. *Experimental design parameters*

Parameter	**Unit**	**Low Level (-1)**	**High Level (+1)**
Leaf:water (LW)	g/ml	1:7	1:15
Extract:$AgNO_3$ solution (EAg)	ml/ml	1:4	1:10
Molarity $AgNO_3$(Mol)	Mol	1	5
Leaf size(LS)	mm	<1	2
Response			
NP amount produced	g		
Dye removal	%		

Plant Biomass and Extraction Procedure

Black collard greens were harvested from gardens in Anatolia's western Black Sea region, Zonguldak, Turkey. First tap water was used to clean the plant leaves, then they were soaked in distilled water to purify any pollutants, and finally dried at ambient temperature in the lab. After drying, the leaves were then chopped and sieved through an 18 mesh sieve. They were then placed in plastic bags until they were used.

12 g of dried leaves were placed to a 250 mL beaker, followed by 180 mL of distilled water to achieve a certain leaf-to-water ratio. For 10-15 minutes, the beaker was whirled in a magnetic stirrer at 100°C until the solution color was turned from yellow to brown. After cooling down, it was passed through a vacuum filter.

Ag Nanoparticle Synthesis and Characterization

Previously prepared plant extracts were reacted with a specific amount of $AgNO_3$ to achieve the necessary ratio. The development of nanoparticles was noticed by a color change from brown to pale yellow and then back to brown after the nanoparticles formed. The nanoparticle formation was determined with a Schimadzu UV-1800 spectrophotometer between 300-700 nm for 24 hours. After the reaction, the reaction solution was dried in an incubator at 105 °C for 24 hours. The beaker was then cleaned with distilled water and vacuum-filtered using filter paper from Whatman No. 1. Filter sheets were dried in an incubator at 105°C for two hours. The characterization of the structure and molecular morphology were achieved by scanning electron microscopy (SEM).

Batch Adsorption Test

Dye removal studies were carried out in batch reactors using 50 mL beakers containing 0.5 mg/L Methylene Blue (MB). The beaker was filled with 0.02 g of AgNP, and the samples were kept under sunlight. After 24 h, samples were taken, and color was measured at 664nm in the spectrophotometer. The methylene blue uptake on the NPs and percentage of removal were calculated by:

$$qe = ((Co - Ct) \times V)/W \quad (1)$$

$$\text{Removal } (\%) = (Co - Ct)/Co \times 100 \quad (2)$$

Here, Co indicates the beginning concentration (mg/L), Ct the concentration at time t (mg/L), V the volume of solution (L), and W the weight of NPs (g).

3. RESULTS AND DISCUSSION

Analysis of Factorial Design

Figure 1 represents synthesized nanoparticles with observed color changes indicating nanoparticle formation and an increase in absorption peaks in the direction of the arrow from 5 min to 24 h.

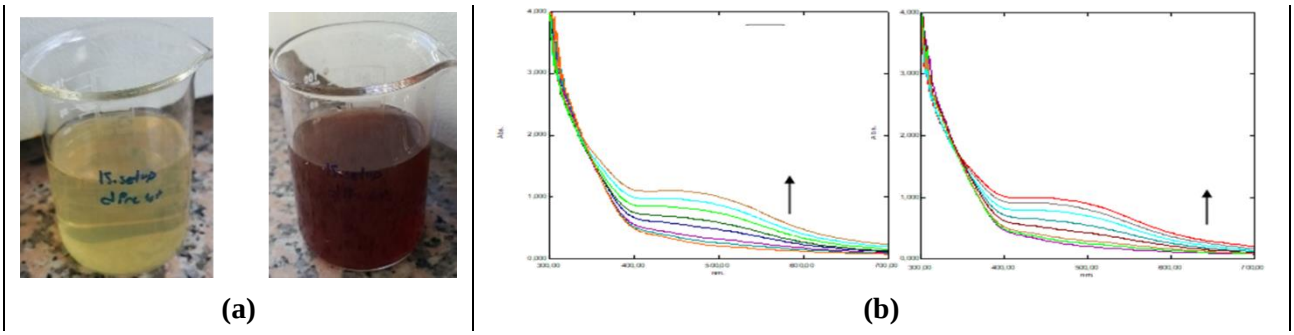

(a) **(b)**

Figure 1. *Color change and absorption peaks during nanopartcile synthesis*
a) *color change from pale yellow to brown* ***b)*** *UV absorption peaks between 5 min-24 h.*

Surface plasmon resonance (SPR) occurs in AgNPs containing free electrons, resulting in the creation of an absorbance band (Noginov et al., 2007). This distinct property enables silver-containing metal nanoparticles to absorb in the ultraviolet-visible (UV-VIS) region. As a result, SPR is a useful instrument for monitoring the reduction of Ag+ ions. Because of surface plasmon resonances, the absorption spectra of AgNPs exhibit maximal absorption within the region of 400-500 nm during the process (Akter et al., 2018; Imanzadeh & Hadi, 2018). When examining the UV spectrum presented in Figure 1, it becomes evident that the band gap corresponding to surface plasmon resonance (SPR) varies within the range of 430-460 nm. This variation in the SPR band gap coincides with the formation of nanoparticles, as observed in the spectrum.

Based on a factorial design of four independent parameters at two levels in triplicate, a total of 48 runs of NP production and dye removal experiments were performed. The responses were given as an averaged mean in Table 2.

Table 2. *Summary of the full factorial design*

Run	Leaf:Water (g/ml)	Extract:$AgNO_3$ (ml/ml)	Mol $AgNO_3$ (mmol)	Leaf Size (mm)	Response (gr NP)	Response Removal (%)
1	1:7	1:4	1	1	0.2165	38.83
2	1:7	1:10	1	1	0.1091	63.91
3	1:15	1:10	1	1	0.1299	45.90
4	1:15	1:4	5	1	0.2567	43.23
5	1:7	1:10	5	1	0.2471	43.54
6	1:7	1:4	1	2	0.2030	44.62
7	1:15	1:4	1	2	0.1676	61.11
8	1:7	1:10	1	2	0.1212	54.44
9	1:15	1:10	1	2	0.0634	
10	1:7	1:4	5	2	0.2968	35.47
11	1:7	1:10	5	2	0.2838	53.16
12	1:15	1:10	5	2	0.2197	49.88
13	1:15	1:4	1	1	0.1888	51.87
14	1:15	1:4	5	2	0.2810	62.67
15	1:7	1:4	5	1	0.3974	56.12
16	1:7	1:4	1	2	0.203	44.62

An ANOVA test has been performed to establish the statistical significance of the model's and variables' fit. Tables 3 and 4 show ANOVA tables for nanoparticulate formation and dye removal. In the ANOVA table, DF indicates the degree of freedom, ADJ SS refers to the sum of squares, ADJ MS indicates mean squares, F represents the distribution factor, and p refers to the significance factor. A statistically significant parameter should have a p-value less than 0.05 at a 95% confidence level. The reaction factor with the highest F value was the most effective. The ANOVA tables reveal that the design model fits the data (p0.05) and that all parameters in nanoparticulate formation and dye removal efficiency are statistically significant, with the exception of the LW ratio, which has a p value of >0.05 in Table 3. The 2-way interactions LW x EAg, LW x Mol, and EAg x Mol, as well as the 3-way interactions LW x EAg x Mol, LW x Mol x LS, and EAg x Mol x LS, all have p-values of 0.05, indicating statistically significant effects. Contributions from two-way and three-way interactions account for 2.65 and 5.84 percent of total contributions, respectively. The term molarity had the highest contribution, with 58.77 for NP production. In the case of dye removal efficiency, all the 2-way and 3-way interactions are statistically significant with a p-value of < 0.05. The prob > F value was greater than 0.050, indicating insignificant terms could be eliminated from the model. Contrary to NP production, the contribution of 2-way and 3-way interactions to the removal response is quite high, 45.42% and 47.11%, respectively.

Table 3. *ANOVA for selected factorial model response of produced nanoparticles*

Source	DF	Adj SS	Adj MS	F-Value	P-Value	Percent Contribution
Model	15	0.307912	0.020527	48.84	0.000	95.94
Linear	4	0.275584	0.068896	163.92	0.000	85.87
LW (Leaf:water)	1	0.020087	0.020087	47.79	0.000	6.26
EAg (Extract:$AgNO_3$)	1	0.065023	0.065023	154.70	0.000	20.26
Mol (Molarity $AgNO_3$)	1	0.188626	0.188626	448.79	0.000	58.77
LS (Leaf Size)	1	0.003810	0.003810	9.06	0.005	1.19
2-Way Interactions	6	0.008520	0.001420	3.38	0.011	2.65
LW*EAg	1	0.002087	0.002087	4.97	0.033	0.65
LW*Mol	1	0.003172	0.003172	7.55	0.010	0.99
LW*LS	1	0.000036	0.000036	0.09	0.771	0.01
EAg*Mol	1	0.002072	0.002072	4.93	0.034	0.65
EAg*LS	1	0.001087	0.001087	2.59	0.118	0.34
Mol*LS	1	0.000204	0.000204	0.48	0.491	0.06
3-Way Interactions	4	0.018744	0.004686	11.15	0.000	5.84
LW*EAg*Mol	1	0.000546	0.000546	1.30	0.263	0.17
LW*EAg*LS	1	0.011187	0.011187	26.62	0.000	3.49
LW*Mol*LS	1	0.004565	0.004565	10.86	0.002	1.42
EAg*Mol*LS	1	0.002478	0.002478	5.90	0.021	0.77
4-Way Interactions	1	0.002064	0.002064	4.91	0.034	0.64
LW*EAg*Mol*LS	1	0.002064	0.002064	4.91	0.034	0.64
Error	31	0.013029	0.000420			4.06
Total	46	0.320942				100.00

The model's R^2 value is 95.94%, which is adequate for describing the observed data. The modified R-squared statistic is 93.98%.

Figure 2 depicts the residuals analysis performed to confirm the ANOVA assumptions. Normal probability plots of standardized residuals fit quite well against the standardized residuals, as seen in the figure, indicating that the model prediction statistically fits the data. Figure 2 also depicts standardized residuals in relation to experimental runs, standardized residuals in relation to estimated values, histogram plots of the standardized residuals, and a normal probability map of the residuals' analysis results. The data showed no trend in the distribution of the standardized residual vs the fitted value, indicating that the constant variance assumption was valid. As a result, both the normality and constant variance assumptions were met.

Table 4. *ANOVA for selected factorial model response of dye removal*

Source	DF	Adj SS	Adj MS	F-Value	P-Value	Percent Contribution
Model	14	3542.25	253.02	10.89	0.000	83.56
Linear	4	719.65	179.91	7.74	0.000	16.98
LW	1	80.92	80.92	3.48	0.072	1.91
EAg	1	173.83	173.83	7.48	0.010	4.10
Mol	1	509.41	509.41	21.92	0.000	12.02
LS	1	491.05	491.05	21.13	0.000	11.58
2-Way Interactions	6	1925.33	320.89	13.81	0.000	45.42
LW*EAg	1	1419.11	1419.11	61.08	0.000	33.48
LW*Mol	1	951.17	951.17	40.94	0.000	22.44
LW*LS	1	173.02	173.02	7.45	0.011	4.08
EAg*Mol	1	403.36	403.36	17.36	0.000	9.51
EAg*LS	1	828.37	828.37	35.65	0.000	19.54
Mol*LS	1	259.38	259.38	11.16	0.002	6.12
3-Way Interactions	4	1996.95	499.24	21.49	0.000	47.11
LW*EAg*Mol	1	1468.75	1468.75	63.21	0.000	34.65
LW*EAg*LS	1	1442.12	1442.12	62.07	0.000	34.02
LW*Mol*LS	1	424.54	424.54	18.27	0.000	10.01
EAg*Mol*LS	1	777.03	777.03	33.44	0.000	18.33
Error	30	697.03	23.23			16.44
Total	44	4239.28				100.00

The model's R^2 value is 83.56%, and the corrected R-squared statistic is 75.88%.

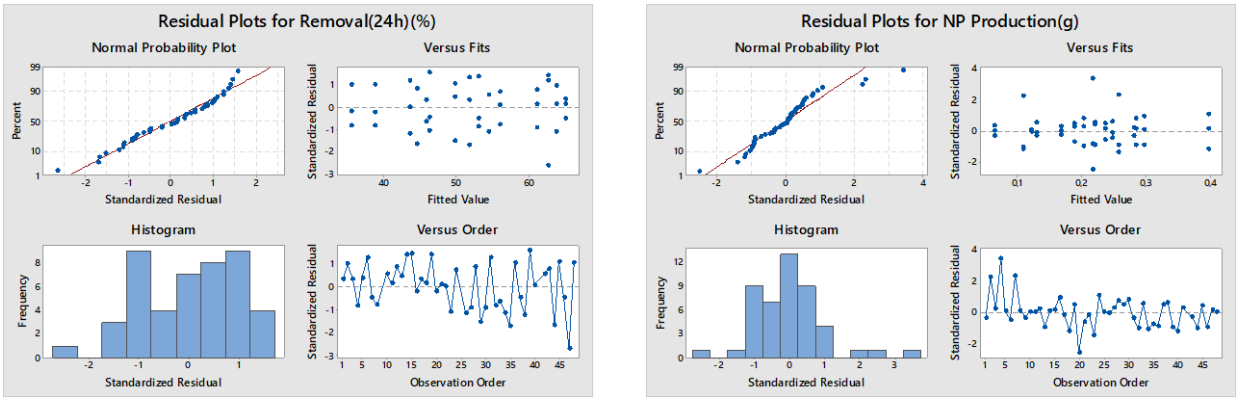

(a) **(b)**

Figure 2. *Analysis of residuals* ***a)*** *for response removal* ***b)*** *for response NP production*

Figures 3 and 4 show the normal probability plots of the standardized effects for NP production and dye removal, respectively, to help analyze each factor and its interaction. There are two distinct regions on each of the two plots: one below 50%, where the factors and their interactions demonstrated significant negative coefficients, and one above 50%, where the factors and their interactions demonstrated significant positive coefficients. When the data in the ANOVA tables is compared to the graphs in Figures 3 and 4, it is apparent that the molarity of $AgNO_3$ is the most important component in the NP formation process. The extract to $AgNO_3$ ratio is the second crucial element. The third important factor is the ratio of leaf to water, and finally, 2-way interactions among LW, EAg, and Mol are important. According to the graphs and ANOVA tables, the variable LS shows a significant adverse impact on NP production. While the two-way interactions between LS and other parameters are insignificant, the three-way interactions between LS and other parameters have a significant negative influence on NP production. The synergical effect of LWxEAgxMol is the most significant term in the dye removal effectiveness of produced nanoparticles, followed by the interaction of EAgxLS and the main influence of Mol. The 2- way interactions of EAgxMol, LWxMol, and LWEAg and the 3-way interactions of LWxMolxLS, EAgxMolxLS, and LWxEAgxLS are also significant terms with negative coefficients.

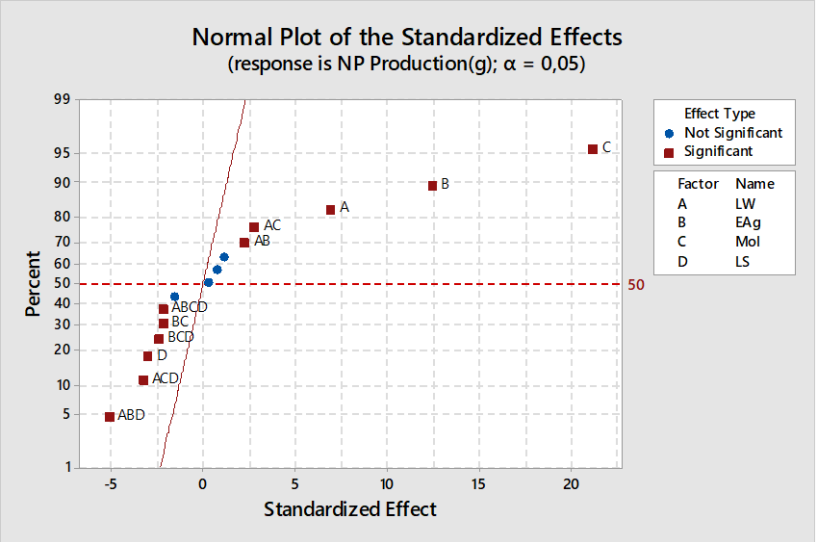

Figure 3. *The standardized effects for NP production*

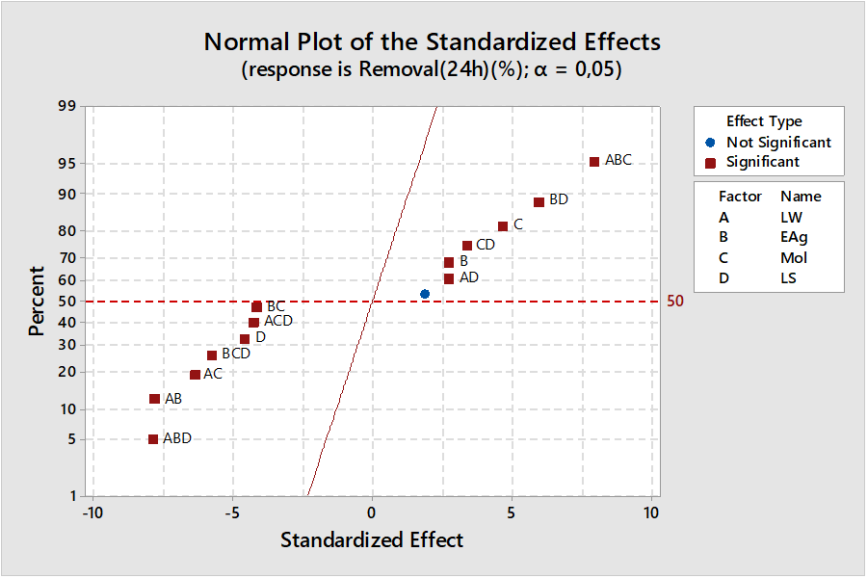

Figure 4. *The standardized effects for dye removal*

Regression equations of the NP generation and dye removal are given together with all of the main and interaction effects of all factors in Equation 1 and Equation 2.

NP Produced (gr)= 0,21359 + 0,02077 LW + 0,03738 EAg + 0,06366 Mol - 0,00905 LS + 0,00670 LW*EAg + 0,00826 LW*Mol + 0,00088 LW*LS - 0,00667 EAg*Mol - 0,00483 EAg*LS + 0,00209 Mol*LS + 0,00342 LW*EAg*Mol - 0,01550 LW*EAg*LS - 0,00990 LW*Mol*LS - 0,00730 EAg*Mol*LS - 0,00666 LW*EAg*Mol*LS (3)

Removal efficiency (24 hour) (%) = 46,927 + 1,836 LW + 2,691 EAg + 4,607 Mol - 4,523 LS - 7,690 LW*EAg - 6,295 LW*Mol + 2,685 LW*LS - 4,100 EAg*Mol + 5,875 EAg*LS + 3,288 Mol*LS + 7,823 LW*EAg*Mol - 7,752 LW*EAg*LS - 4,206 LW*Mol*LS - 5,690 EAg*Mol*LS (4)

Table 5 displays the outcomes of the experimental data optimization. The factors mol $AgNO_3$ and leaf size are the same for boyh responses. At the optimum conditions for maximum NP production (LW 1:7; EAg 1:4), a removal efficiency of 56.12% was achieved. When the ratio of leaf to water was increased to 1:15 and the extract to $AgNO_3$ to 1:10, the removal efficiency reached a maximum value of 65.52%.

Table 5*. Optimum AgNPs synthesis conditions*

Responses	Leaf:Water (LW)	Extract:$AgNO_3$ (EAg)	Mol $AgNO_3$ (Mol)	Leaf Size (LS)	Maximum Yield
NP Production (g)	1:7	1:4	5	<1	0.397
Dye Removal (%)	1:15	1:10	5	<1	65.52

A fast response rate, a short contacting time, and a high capacity for adsorption are essential for an efficient adsorption process. Adsorption features are better understood when reaction rate equations are used to explain the variance in the effective number of functioning sites on the adsorbent surface throughout adsorption (Liu et al., 2019). Equations 5-6 provide the linear form of the pseudo-first-order and pseudo-second-order kinetic models, respectively.

$$ln\,(qe - qt) = lnqe - k_1 t \quad (5)$$

$$\frac{t}{qt} = \frac{1}{k_2\, qe^2} + \frac{1}{qe} \quad (6)$$

Here k_1 is the pseudo-first-order rate constant, k_2 is the pseudo-second-order rate constant, qe is the quantity of dye adsorbed at equilibrium per unit weight of the adsorbent (mg g^{-1} min^{-1}) and qt is the amount of solute adsorbed (mg $g^{-1}min^{-1}$) at a time 't', and t is the time (min).

Figure 5 presents linear fits of the pseudo-first order and pseudo-second order kinetics, and Table 6 presents the derived corresponding factors. The elimination of methylene blue best fits the pseudo-first-order model under the conditions required to optimize NP production, with an R^2 of 0.979. Although the R^2 of pseudo first order and pseudo second order reaction kinetics are nearly the same, pseudo second order is slightly higher (0.981) for NPs produced under optimal conditions to enhance dye elimination. The rate constants of pseudo-first-order reactions are greater than those of pseudo-second-order reactions. The pseudo-first-order approach implies that the adsorption rate corresponds to the difference between the saturation concentration (qe) and the rate of solute uptake with time t (qt). The pseudo-second-order equation, on the contrary, assumes that the sorption is governed by a chemical adsorption process governed by electron sharing or transfer (Zhang et al., 2016). Bhargavi et al. (2015) studied the color black G (CBG) removal with ZnO nanoparticles, and they claim that the adsorption was best explained by the pseudo-first-order kinetics. MgO NPs adsorbed two different dyes, Reactive Blue 19 and Reactive Red, 198, representing azo and anthraquinone dyes. The kinetic tests of both dyes revealed a pseudo-second-order model (Moussavi & Mahmoudi, 2009). The pseudo-second-order kinetic method was used for removing the anionic dye known as methyl orange using Co_3O_4 nanoparticles (Uddin & Baig, 2019).

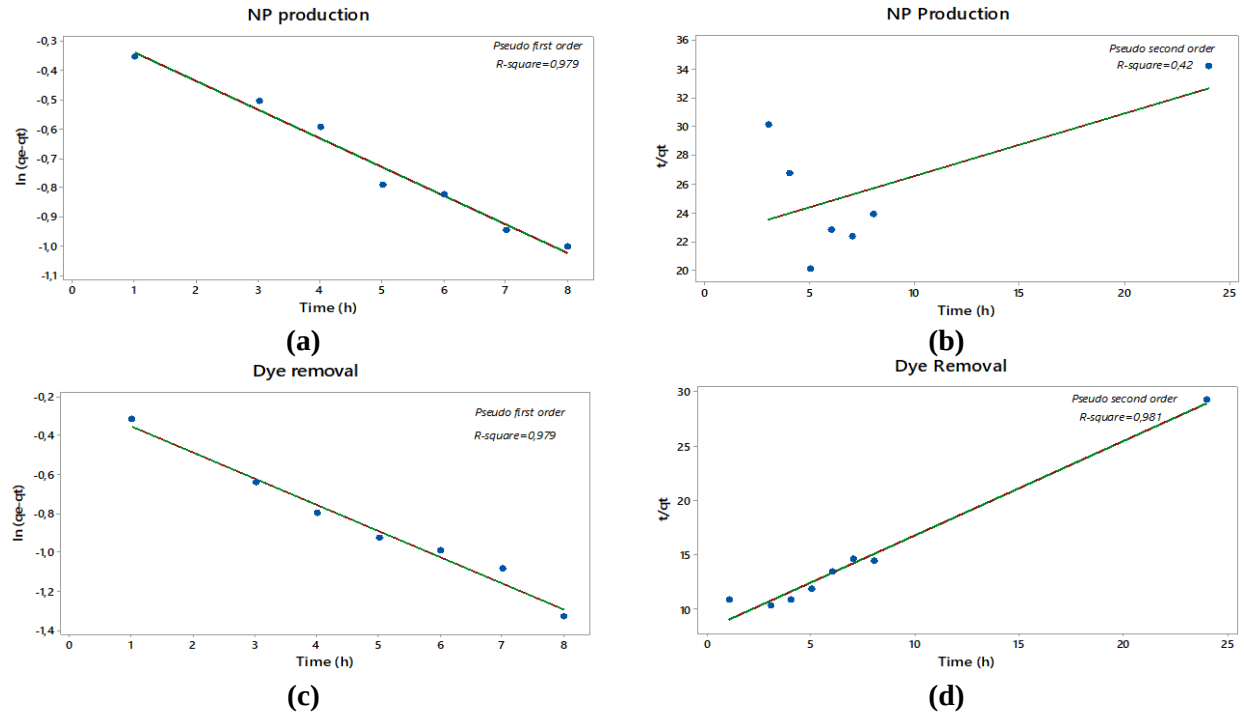

Figure 5. *Linear form of the reaction models fitted for the responses NP production* ***a)*** *pseudo first order* ***b)*** *pseudo second order and dye removal* ***c)*** *pseudo first order* ***d)*** *pseudo second order*

Table 6. *Reaction rate constants for pseudo-first-order and pseudo-second-order model*

	Pseudo first order		**Pseudo second order**	
	qe (mg/g)	**K1 (min^{-1})**	**qe(mg/g)**	**K2 (min^{-1})**
Maximum NP production	0,79	0,01224	2,29	0,0086
Maximum dye removal	0,80	0,01675	1,15	0,0092

Characterization of the produced nanoparticles

The scanning electron microscope (SEM) technique has been performed to identify the morphological structure of the silver nanoparticles. The SEM images of the particles produced under the optimized conditions of response NP production and dye removal are given in Figure 6. The figures show that the produced nanoparticles are unevenly distributed in size and have irregular shapes.

The particle size distribution of NPs optimized for dye removal is wide, based on SEM size measurements, showing the presence of smaller particles that contribute to a higher removal effectiveness. The information provided suggests that there is a difference in the size of NPs observed under 100000x magnification between the production experiments and the dye removal experiments. The size of the NPs observed during the production experiments was 71-219 µm, while the size of the NPs detected during the dye removal studies was 49-75 µm. The smaller NPs with a wider size distribution can provide more surface area for interactions with the dye molecules, leading to a higher removal efficiency. Silver nanoparticles with a large surface area act as a fitting catalyst for the electron transfer reaction of methylene blue molecules (Vidhu & Philip, 2014; VenkataRao et al., 2020)

Particle size and surface area analysis was conducted by a mastersizer. This analytical approach characterizes particle size distribution and gives useful information about the surface area of nanoparticles. Plant-mediated silver nanoparticles are often polydispersed due to the existence of a variety of reducing compounds in the plant extract. This results significant heterogeneity in shape and size of the nanoparticles (Bala & Rani, 2020).

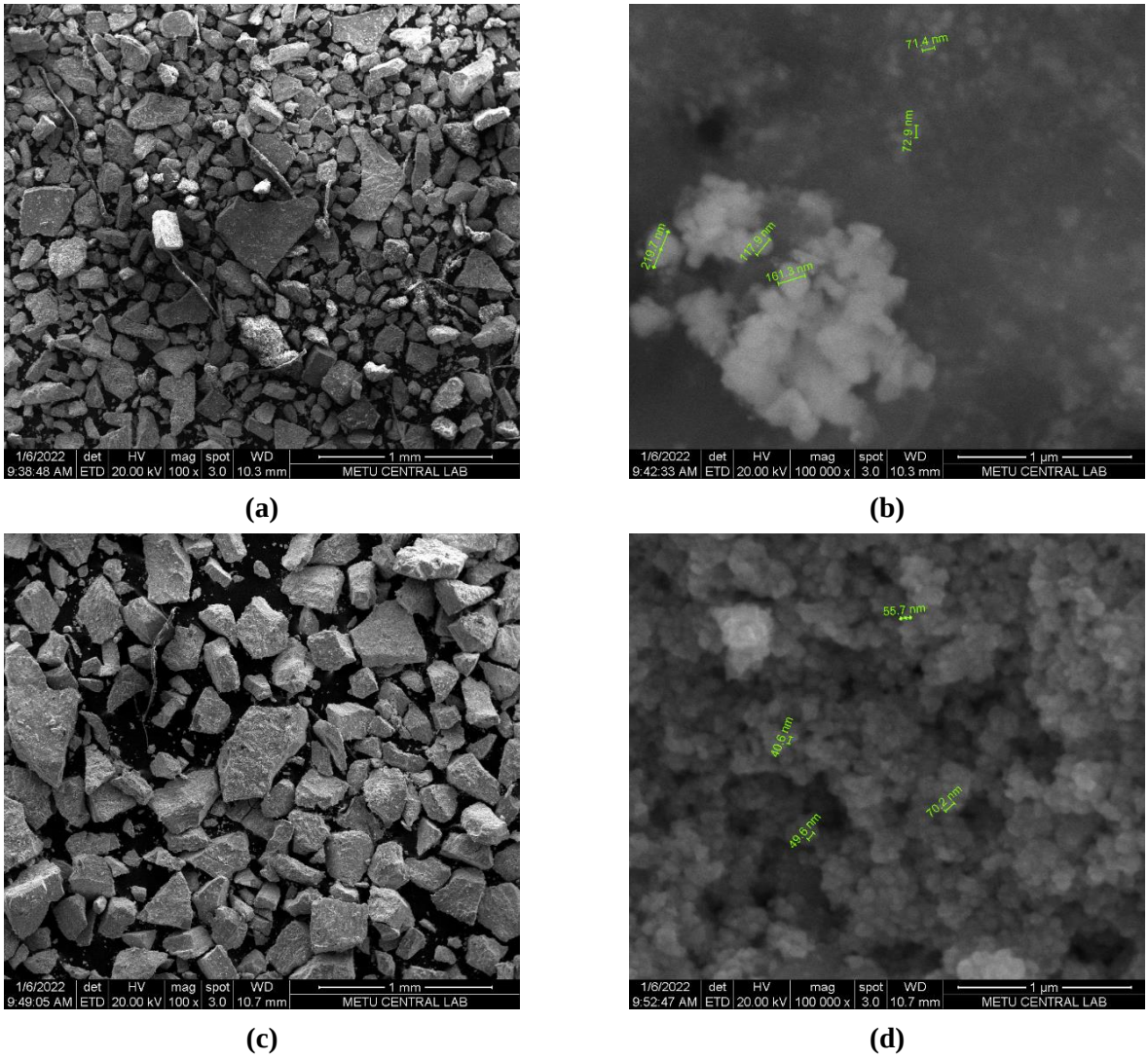

Figure 6. *SEM images of the NPs produced at the optimum conditions of* ***a)****,* ***b)*** *NP production* ***c)****,* ***d)*** *dye removal*

Figure 7 shows that under conditions where nanoparticle production is maximized, the particle sizes exhibit a narrower distribution within a specific range. However, under conditions where the dye removal efficiency is maximized, the particle size variation spans a wider range. The specific surface areas are measured as 0.0833 and 0.202 m^2/g for NP production and dye removal, respectively. The existence of smaller particles under dye removal circumstances leads to a more even distribution of particle sizes, which gives a larger surface area. This increased surface area allows for greater dye removal effectiveness. The smaller particles provide greater activity locations for dye molecules to interact with, increasing the overall efficacy of the removal process.

Researchers have investigated the parameters influencing nanoparticle synthesis, which include pH, extract concentration, and metal salt concentration. The relationship between the morphological properties of nanoparticles and synthesis conditions was evaluated. Venugobal and Anandalakshmi (2016) have produced silver nanoparticles from Commiphora caudata leaf extract. Their research concludes that, the absorbance of the generated nanoparticles increases with the percentage of the extract of leaves. The maximum absorbance was recorded at increased leaf extract concentrations (5 ml). Because of the higher leaf concentrate, symmetrical nanoparticles were generated (Venugobal & Anandalakshmi, 2016). A different study utilised Acalypha hispida to modify the physicochemical properties of the silver nanoparticles. Silver nanoparticles produced within 20-50 nm have a spherical shape that is reliant on the quantity of plant extract (Sithara et al., 2017). It has been found that when the volume of plant extract increases, the absorption peak changes towards longer wavelengths, indicating the existence of large-sized nanoparticles (Rajput et al., 2020). As a result, bigger particles were generated in this investigation as the concentration of the reactive extract of plants rose.

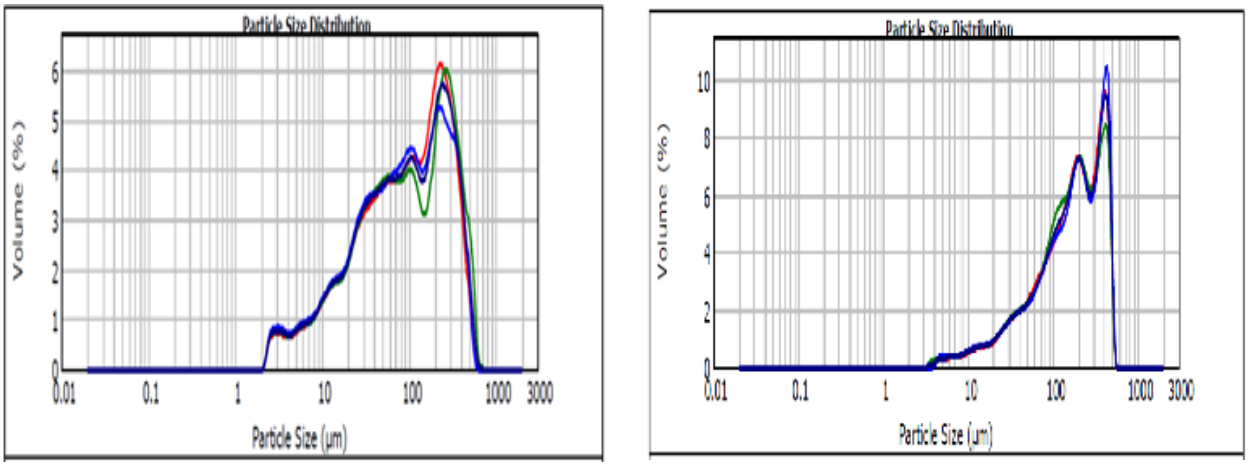

(a) **(b)**

Figure 7. *Particle size partitioning of the NPs produced at the optimum conditions of* ***a)*** *NP production,* ***b)*** *dye removal*

Silver ion concentration has a considerable influence on the size, shape, and also the extent of silver nanoparticle production. *Syzygium cumini* (*S.cumini*) fruit extract was utilized to synthesize biogenic new silver nanoparticles (AgNP) in a single pot, and it was discovered that there was a direct proportional relationship between metal salt concentration and nanoparticle creation. They discovered a unique SPR band at natural concentrations (0.5 mM-1 mM). As the salt concentration was increased over 1 mM, however, a red (bathochromic) shifting appeared, which suggests an appearance of large-sized and polydisperse nanoparticles (Parmar et al., 2019). Increasing the concentration of $AgNO_3$ was found to increase the synthesis of AgNP. A deformed peak was observed above a concentration of 5 mM of $AgNO_3$. At increasing $AgNO_3$ concentrations, absorption spectra switched to longer wavelengths (426-450 nm), demonstrating increased AgNP production (red-shifted) (Rajput et al., 2020). Saini et al. (2019) discovered during their research on C. corylifolium that the synthesis rate of AgNPs increased with higher concentrations of $AgNO_3$, and the absorption spectra shifted towards longer wavelengths (Abdelghany et al., 2018). In this study, the nanoparticles' dominant size was found to be greater than 70 nm both for NP production and dye removal because the experimental design optimized the concentration of $AgNO_3$ to 5mM.

4. CONCLUSION

The current study used a full factorial design (FFD) to optimize the green synthesis parameters of silver nanoparticle (AgNP) production in order to increase dye removal efficiency. The study has evaluated four parameters, namely the ratio of water to plant leaf, the ratio of extract to AgNO3, the molarity of $AgNO_3$, and the plant leaf size, at two levels each, to determine their effect on the amount of synthesized AgNPs and dye removal efficiency. According to the findings, the factors had a substantial impact on AgNP production and dye removal efficiency. The characterization of synthesized NP were carried out by SEM and mastersizer analysis The analysis confirmed that the sizes of synthesized AgNPs are different for two conditions, which in turn results in differences in dye removal efficiencies. The dye removal efficiency of green-synthesized AgNPs is considerably high, even it was applied at a low dosage (0.02 g). The kinetic analysis confirmed that methylene blue adsorption on AgNPs follows pseudo-first-order reaction kinetics with concentration difference as a driving force. Overall, the research presents a useful framework for optimizing green AgNP production and their prospective uses in water treatment.

ACKNOWLEDGEMENT

The authors acknowledge financial support from the BAP project (2021-77047330-01). The authors also express their gratitude towards Zonguldak Bulent Ecevit University for their financial support and assistance in preparing this manuscript.

CONFLICT OF INTEREST

The authors declare no conflict of interest.

REFERENCES

Abdelghany, T. M., Al-Rajhi, A. M. H., Al Abboud, M. A., Alawlaqi, M. M., Ganash Magdah, A., Helmy, E. A. M., & Mabrouk, A. S. (2018). Recent Advances in Green Synthesis of Silver Nanoparticles and Their Applications: About Future Directions. A Review. *BioNanoScience*, *8*(1), 5-16. doi:10.1007/s12668-017-0413-3

Akter, M., Rahman, Md. M., Ullah, A. K. M. A., Sikder, Md. T., Hosokawa, T., Saito, T., & Kurasaki, M. (2018). Brassica rapa var. japonica Leaf Extract Mediated Green Synthesis of Crystalline Silver Nanoparticles and Evaluation of Their Stability, Cytotoxicity and Antibacterial Activity. *Journal of Inorganic and Organometallic Polymers and Materials*, *28*(4), 1483-1493. doi:10.1007/s10904-018-0818-7

Bala, A., & Rani, G. (2020). A review on phytosynthesis, affecting factors and characterization techniques of silver nanoparticles designed by green approach. *International Nano Letters*, *10*(3), 159-176. doi:10.1007/s40089-020-00309-7

Bhargavi, R. J., Maheshwari, U., & Gupta, S. (2015). Synthesis and use of alumina nanoparticles as an adsorbent for the removal of Zn(II) and CBG dye from wastewater. *International Journal of Industrial Chemistry*, *6*(1), 31-41. doi:10.1007/s40090-014-0029-1

Çimen, B., Şengül, S., Ergüt, M., & Özer, A. (2019). Green Synthesis and Characterization of CuO Nanoparticles: Telon Blue AGLF and Methylene Blue Adsorption. Sinop University Journal of Natural Sciences, *4*(1), 1-20. doi:10.33484/sinopfbd.315643

David, L., & Moldovan, B. (2020). Green Synthesis of Biogenic Silver Nanoparticles for Efficient Catalytic Removal of Harmful Organic Dyes. *Nanomaterials*, *10*(2), 202. doi:10.3390/nano10020202

Golli, R., Thummaneni, C., Pabbathi, D. D., Srungarapu, T., Jayasri, G., & Vangalapati, M. (2023). *Silver nanoparticles synthesized by Brassica oleracea (Broccoli) acting as antifungal agent against Candida albicans*. In: M. Seenuvasan, & D. M. Sangeetha (Eds.), Proceedings of the Second Global Conference on Recent Advances in Sustainable Materials 2022. Materials Today: Proceedings, (vol. 80, part 2, pp. 1495-1500). doi:10.1016/j.matpr.2023.01.284

Imanzadeh, G., & Hadi, R. (2018). Brassica Oleraceae, A Versatile Plant For Green Synthesis of Silver Nanoparticles. *Iranian Chemical Communication*, *6*(1), 70-77.

Iravani, S. (2011). Green synthesis of metal nanoparticles using plants. *Green Chemistry*, *13*(10), 2638-2650. doi:10.1039/C1GC15386B

Jeevanandam, J., Chan, Y. S., & Danquah, M. K. (2016). Biosynthesis of metal and metal oxide nanoparticles. *ChemBioEng Reviews*, *3*(2), 55-67. doi:10.1002/cben.201500018

Jiang, C., Wang, X., Qin, D., Da, W., Hou, B., Hao, C., & Wu, J. (2019). Construction of magnetic lignin-based adsorbent and its adsorption properties for dyes. *Journal of Hazardous Materials*, *369*, 50-61. doi:10.1016/j.jhazmat.2019.02.021

Kumar Das, P., Mohanty, C., Krishna Purohit, G., Mishra, S., & Palo, S. (2022). Nanoparticle assisted environmental remediation: Applications, toxicological implications and recommendations for a sustainable environment. *Environmental Nanotechnology, Monitoring & Management*, *18*, 100679. doi:10.1016/j.enmm.2022.100679

Lee, H. U., Lee, S. C., Lee, Y.-C., Vrtnik, S., Kim, C., Lee, S., Lee, Y. B., Nam, B., Lee, J. W., Park, S. Y., Lee, S. M., & Lee, J. (2013). Sea-urchin-like iron oxide nanostructures for water treatment. *Journal of Hazardous Materials*, *262*, 130-136. doi:10.1016/j.jhazmat.2013.08.014

Liu, X., Tian, J., Li, Y., Sun, N., Mi, S., Xie, Y., & Chen, Z. (2019). Enhanced dyes adsorption from wastewater via Fe3O4 nanoparticles functionalized activated carbon. *Journal of Hazardous Materials*, *373*, 397-407. doi:10.1016/j.jhazmat.2019.03.103

Min, K. H., Shin, J. W., Ki, M.-R., & Pack, S. P. (2023). Green synthesis of silver nanoparticles on biosilica diatomite: Well-dispersed particle formation and reusability. *Process Biochemistry*, *125*, 232-238. doi:10.1016/j.procbio.2022.12.018

Moussavi, G., & Mahmoudi, M. (2009). Removal of azo and anthraquinone reactive dyes from industrial wastewaters using MgO nanoparticles. *Journal of Hazardous Materials*, *168*(2–3), 806-812. doi:10.1016/j.jhazmat.2009.02.097

Ngoc, P. K., Mac, T. K., Nguyen, H. T., Viet, D. T., Thanh, T. D., Van Vinh, P., Phan, B. T., Duong, A. T., & Das, R. (2022). Superior organic dye removal by $CoCr_2O_4$ nanoparticles: Adsorption kinetics and isotherm. *Journal of Science: Advanced Materials and Devices*, *7*(2), 100438. doi:10.1016/j.jsamd.2022.100438

Nie, P., Zhao, Y., & Xu, H. (2023). Synthesis, applications, toxicity and toxicity mechanisms of silver nanoparticles: A review. *Ecotoxicology and Environmental Safety*, *253*, 114636. doi:10.1016/j.ecoenv.2023.114636

Noginov, M. A., Zhu, G., Bahoura, M., Adegoke, J., Small, C., Ritzo, B. A., Drachev, V. P., & Shalaev, V. M. (2007). The effect of gain and absorption on surface plasmons in metal nanoparticles. *Applied Physics B: Lasers and Optics*, *86*(3), 455-460. doi:10.1007/s00340-006-2401-0

Rastogi, A., Zivcak, M., Sytar, O., Kalaji, H. M., He, X., Mbarki, S., & Brestic, M. (2017). Impact of Metal and Metal Oxide Nanoparticles on Plant: A Critical Review. *Frontiers in Chemistry*, *5*, 78. doi:10.3389/fchem.2017.00078

Rajput, S., Kumar, D., & Agrawal, V. (2020). Green synthesis of silver nanoparticles using Indian Belladonna extract and their potential antioxidant, anti-inflammatory, anticancer and larvicidal activities. *Plant Cell Reports*, *39*(7), 921-939. doi:10.1007/s00299-020-02539-7

Parmar, A., Kaur, G., Kapil, S., Sharma, V., Choudhary, M. K., & Sharma, S. (2019). Novel biogenic silver nanoparticles as invigorated catalytic and antibacterial tool: A cleaner approach towards environmental remediation and combating bacterial invasion. *Materials Chemistry and Physics*, *238*, 121861. doi:10.1016/j.matchemphys.2019.121861

Silva, L. P., Reis, I. G., & Bonatto, C. C. (2015). Green Synthesis of Metal Nanoparticles by Plants: Current Trends and Challenges. In: V. A. Basiuk & E. V Basiuk (Eds.), *Green Processes for Nanotechnology: From Inorganic to Bioinspired Nanomaterials*, (pp. 259-275). Springer. doi:10.1007/978-3-319-15461-9_9

Sithara, R., Selvakumar, P., Arun, C., Anandan, S., & Sivashanmugam, P. (2017). Economical synthesis of silver nanoparticles using leaf extract of Acalypha hispida and its application in the detection of Mn(II) ions. *Journal of Advanced Research*, *8*(6), 561-568. doi:10.1016/j.jare.2017.07.001

Uddin, M. K., & Baig, U. (2019). Synthesis of Co_3O_4 nanoparticles and their performance towards methyl orange dye removal: Characterisation, adsorption and response surface methodology. *Journal of Cleaner Production*, *211*, 1141-1153. doi:10.1016/j.jclepro.2018.11.232

VenkataRao, P., SaiTarun, G., Govardhani, Ch., Manasa, B., Joy, P. J., & Vangalapati, M. (2020). *Biosorption of congo red dye from aqueous solutions using synthesized silver nano particles of Grevillea robusta : Kinetic studies*. In: S. K. Singh, E. T. Akinlabi, K. Kumar, J. P. Davim, & K. K. Saxena (Eds.), Proceedings of the 10th International Conference of Materials Processing and Characterization. Materials Today: Proceedings, (vol. 26, part 2, pp. 3009-3014). doi:10.1016/j.matpr.2020.02.626

Venugobal, J., & Anandalakshmi, K. (2016). Green Synthesis of Silver Nanoparticles Using Commiphora caudata Leaves Extract and the Study of Bactericidal Efficiency. *Journal of Cluster Science*, *27*(5), 1683-1699. doi:10.1007/s10876-016-1032-9

Vidhu, V. K., & Philip, D. (2014). Catalytic degradation of organic dyes using biosynthesized silver nanoparticles. *Micron*, *56*, 54-62. doi:10.1016/j.micron.2013.10.006

Wang, J., Zhang, Q., Shao, X., Ma, J., & Tian, G. (2018). Properties of magnetic carbon nanomaterials and application in removal organic dyes. *Chemosphere*, *207*, 377-384. doi:10.1016/j.chemosphere.2018.05.109

Yaghoobi, M., Asjadi, F., & Sanikhani, M. (2023). A facile one-step green hydrothermal synthesis of paramagnetic Fe3O4 nanoparticles with highly efficient dye removal. *Journal of the Taiwan Institute of Chemical Engineers*, *144*, 104774. doi:10.1016/j.jtice.2023.104774

Zhang, F., Chen, X., Wu, F., & Ji, Y. (2016). High adsorption capability and selectivity of ZnO nanoparticles for dye removal. *Colloids and Surfaces A: Physicochemical and Engineering Aspects*, *509*, 474-483. doi:10.1016/j.colsurfa.2016.09.059